J. Micromech. Microeng. **10** (2000) 452–458. Printed in the UK PII: S0960-1317(00)11946-1

A laterally driven symmetric micro-resonator for gyroscopic applications

Yoon Shik Hong†, Jong Hyun Lee‡ and Soo Hyun Kim†

† Department of Mechanical Engineering, Korea Advanced Institute of Science and Technology, Taejon 305-701, Korea
‡ Department of Mechatronics, Kwangju Institute of Science and Technology, Kwangju, 500-712, Korea

E-mail: kimsh@sorak.kaist.ac.kr and jonghyun@kjist.ac.kr

Received 18 February 2000, in final form 10 May 2000

Abstract. Conventional microgyroscopes of the vibrating type require resonant frequency tuning of the driving and sensing modes to achieve high sensitivity. These tuning conditions depend on each microgyroscope fabricated, even though the microgyroscopes are identically designed. A new micromachined resonator, which is applicable to microgyroscopes with self-tuning characteristics, is presented. Since the laterally driven two-degrees-of-freedom resonator was designed as a symmetric structure with identical stiffness in two orthogonal axes, the resonator is applicable to vibrating microgyroscopes, which do not need mode tuning. A dynamic model of the resonator was derived considering gyroscopic applications. The dynamic model was evaluated by experimental comparison with fabricated resonators. The resonators were fabricated using a simple process of a single polysilicon layer deposited on an insulator layer.

The feasibility of the resonator as a vibrating microgyroscope with self-tuning capability is discussed. The fabricated resonators of a particular design have process-induced non-uniformities that cause different resonant frequencies. For several resonators, the standard deviations of the driving and sensing resonant frequencies were as high as 1232 and 1214 Hz, whereas the experimental average detuning frequency was 91.75 Hz. The minimum detuned frequency was 68 Hz with 0.034 mV s^{-1} sensitivity. The sensitivity of the microgyroscope was low due to process-induced non-uniformity; however, the angular rate bandwidth was wide. This resonator could be successfully applicable to a vibrating microgyroscope with high sensitivity, if improvements in uniformity of the fabrication process are achieved. Further developments in improved integrated circuits are expected to lower the noise level even more.

(Some figures in this article are in colour only in the electronic version; see www.iop.org)

1. Introduction

Because of their low cost, small size and high sensitivity, micromachined gyroscopes are receiving increasing attention. Recently, microgyroscopes have been applied in many fields in view of their precise angular motion detection. Most micromachined gyroscopes are of the vibrating type. Electrostatic comb driving and capacitive sensing of charges are popular in both driving and sensing methods [1–4]. It should be mentioned that conventional vibrating microgyroscopes require tuning of both driving and sensing mode resonant frequencies to attain high sensitivity.

The resonator presented in this study was produced for microgyroscopic application. The microgyroscope using the resonator differs from conventional ones in terms of the mechanical design and fabrication process. In terms of the fabrication, a simple process in which a single polysilicon layer is applied on an insulator layer is presented. In terms of the mechanical design, an idea of a vibrating gyroscope with minimized effort for the tuning of resonant modes is presented. In the fabrication process of vibrating microgyroscopes, process-induced non-uniformity is inevitable; hence, a detuning process of vibrating modes is carried out. The presented vibrating microgyroscope of symmetric structure about the x- and y-axes can minimize mode detuning. In this work a dynamic model of the resonator is derived by considering the gyroscopic application, and the model is evaluated experimentally by comparison with fabricated resonators. The validity of the gyroscopic application, including the self-tuning characteristics, is also evaluated through experiment.

0960-1317/00/030452+07$30.00

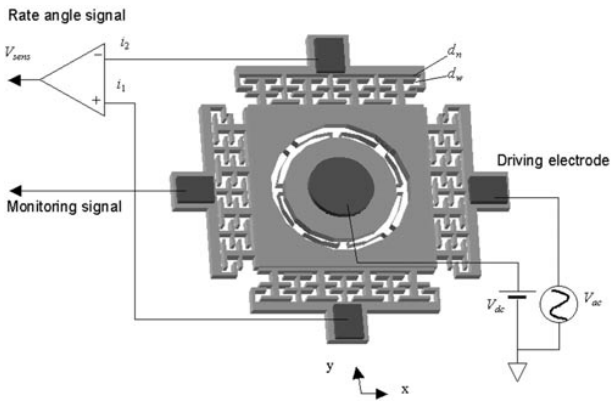

Figure 1. A laterally vibrating resonator, which is symmetric about the x- and y-axes, and its circuit configuration for gyroscopic application.

2. Laterally driven resonator with two degrees of freedom

Figure 1 shows a schematic diagram of a laterally driven resonator with two degrees of freedom (2DOF), which is symmetric about two perpendicular axes, x and y. A circular anchor is located at the center of the overall structure; a vibrating square-shaped mass is supported by eight curved-beam springs, which connect the vibrating mass and the anchor. Since the eight curved springs are also symmetrically configured about the two axes, the overall spring system ideally has the same stiffness in the x and y directions of motion. The resonator is designed with the same stiffness in x and y motions, but not in motions in the z direction, tilting and rotation. Because the motions in the x and y directions are also designed to have far lower stiffness than other motions, the resonator is named 'a laterally driven 2DOF resonator with fundamental vibrations in the x and y directions'. On the four sides of the structure, driving and sensing electrodes of identical shape are configured to be symmetrical about the x- and y-axes. On the four sides of the vibrating mass there are multiple cantilevers that face other cantilevers on the four electrodes and the cantilever sidewalls facing each other are sensitive to electrical charges. Finally, the cantilevers on the vibrating mass and on the electrodes are arranged with alternating narrow and wide gaps.

Comb-driving and parallel plate capacitive sensing are the major methods of driving and sensing in conventional vibrating microgyroscopes. Microgyroscopes of this type have detuning characteristics due to process uncertainties. The laterally driven resonator with 2DOF presented here is designed for a self-tuned vibrating microgyroscope.

Even if identically designed resonators are fabricated on the same wafer, they cannot have the same resonant frequency due to process-induced non-uniformities that cause differences in fabricated dimensions. Since resonators located far from each other will have less uniform dimensions than resonators located near each other, the resonant frequencies of fabricated resonators are generally different, in accordance with their relative positions on the wafer. The resonant frequencies of resonators are mostly determined by the width of beam springs; the practical tolerance in width during fabrication process is about 10%.

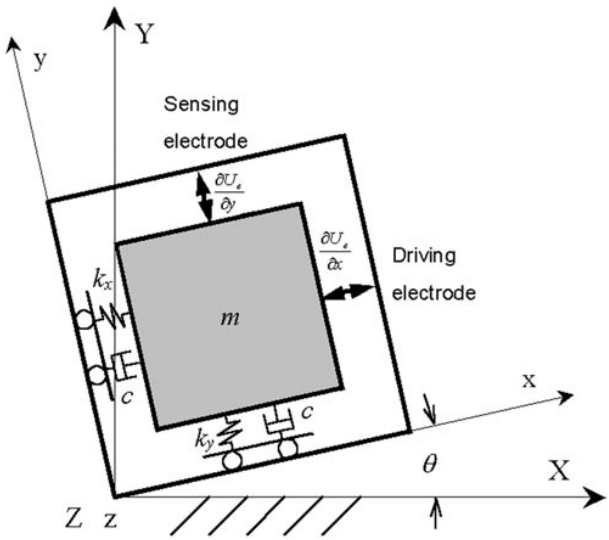

Figure 2. Simplified lumped mass model of a vibrating microgyroscope.

For a mechanically decoupled microgyroscope, the driving and sensing motions of gyroscope have to be perpendicular to each other. For highly sensitive micro-gyroscopes the spring dimensions of the two modes have to be uniformly fabricated in spite of the 10% process tolerance, by locating mode springs as close as possible. Therefore the spring system becomes symmetric about the x- and y-axes.

The schematic diagram of the circuit presented in figure 1 illustrates the gyroscopic application of the laterally driven 2DOF resonator. A dc voltage is provided to the vibrating mass by connecting the metal pad on the circular anchor with a dc voltage source. The vibrating mass is excited in the x direction by providing an ac voltage to the right electrode in figure 1. The right electrode is the driving electrode, while the left is the monitoring electrode for the driving vibration (vibration in the x direction is the driving mode vibration). Any angular motion with an axis of rotation perpendicular to the plane of the substrate causes a Coriolis force creating a sensing mode vibration, i.e. vibration in the y direction. The electrodes at the upper and lower sides of the gyroscope differentially detect current from variation of the electrostatic charge due to such vibrations; the current is then amplified to the sensing signal which is proportional to the angular rate of change.

3. Dynamic model of the microgyroscope

3.1. Equation of motion of the microgyroscope

A simplified lumped mass model of the microgyroscope is shown in figure 2. The model consists of a vibrating mass m, two spring-damper systems and parallel sidewall type electrodes; the electrodes consist of a driving electrode, a monitoring electrode and sensing electrodes. The microgyroscope is attached to a rotating reference frame xyz, which rotates with respect to the fixed reference frame XYZ about axis Z, which is coaxial to axis z. There have been many studies on dynamic models of comb-drive

type microgyroscopes [5–7], but to the authors' knowledge, microgyroscopes with parallel sidewall type driving have not been widely researched.

The equations of motion for the microgyroscope can be obtained using the Lagrange equation, as follows:

$$m\ddot{x} + c\dot{x} + (k_x - m\dot{\theta}^2)x - my\ddot{\theta} - 2m\dot{y}\dot{\theta} + \frac{\partial U_e}{\partial x} = 0 \quad (1a)$$

$$m\ddot{y} + c\dot{y} + (k_y - m\dot{\theta}^2)y + mx\ddot{\theta} + 2m\dot{x}\dot{\theta} + \frac{\partial U_e}{\partial y} = 0 \quad (1b)$$

where U_e is electrostatic potential energy; y, x and θ are the respective displacements in the x, y and angular directions; k_x and k_y are constants; and m is the mass. The vibrating amplitude of m in the y direction is much smaller than that in the x direction; the angular velocity and angular acceleration are much smaller than the resonant frequencies. Therefore, the terms of angular accelerations and centripetal forces are assumed to be negligible, and so is the Coriolis force acting on the x-axis. Defining $\dot{\theta}$ as Ω and using the above assumptions, the equations of motion can be simplified as

$$m\ddot{x} + c\dot{x} + k_x x + \frac{\partial U_e}{\partial x} = 0 \quad (2a)$$

$$m\ddot{y} + c\dot{y} + k_y y + \frac{\partial U_e}{\partial y} = 2m\dot{x}\Omega. \quad (2b)$$

The electrostatic forces acting on each axis do not appear yet in these equations. The electrostatic potential energy can be obtained by understanding the geometric configuration of the electrodes and the structure. As shown in the driving and monitoring electrodes in figure 1, the voltage difference between the parallel sidewall electrodes is V_{dc}, and an ac voltage v_{ac} is supplied from the driving electrode. Partial differentiation of the electrostatic energy by the displacement x, gives the electrostatic driving force of the x-axis as

$$\frac{\partial U_e}{\partial x} = -\varepsilon A_s V_{dc}^2 \left\{ \frac{d_n x}{(d_n^2 - x^2)^2} + \frac{d_w x}{(d_w^2 - x^2)^2} \right\} - \frac{\varepsilon A_s V_{dc}}{2} \left\{ \frac{1}{(d_n - x)^2} - \frac{1}{(d_w + x)^2} \right\} v_{ac} \quad (3)$$

where ε is the permittivity of air, A_s is the electrostatic area and d_n and d_w are the narrow and wide electrode gaps, respectively. A_s is half of the total electrostatic area, which in turn is the sum of the multiple cantilever side areas, and the values of d_w's and d_n's in the driving electrode configuration can be estimated using the electrostatic area A_s. As shown in figure 1, there is only a voltage difference, V_{dc}, between the sensing electrodes and the vibrating structure. Thus, partial differentiation of the electrostatic energy by the displacement y, gives the electrostatic force in the y direction as

$$\frac{\partial U_e}{\partial y} = -\varepsilon A_s V_{dc}^2 \left\{ \frac{d_n y}{(d_n^2 - y^2)^2} + \frac{d_w y}{(d_w^2 - y^2)^2} \right\}. \quad (4)$$

Since the displacement y of the sensing mode is so much smaller than d_n so as to be negligible, it is possible to approximate equation (4) as

$$\frac{\partial U_e}{\partial y} \approx -\left(\frac{\alpha^3 + 1}{\alpha^3} \right) \frac{\varepsilon A_s V_{dc}^2}{d_n} y \equiv -k_e y \quad (5)$$

where α is d_w/d_n, and k_e is defined as the electrostatic-elastic coefficient.

3.2. Driving and sensing modes of the microgyroscope

From equations (2*a*) and (3), the nonlinear equation of motion of the microgyroscope in the driving mode can be rewritten as

$$m\ddot{x} + c\dot{x} + k_x x - \left\{ \frac{\varepsilon A_s V_{dc}^2 d_n}{(d_n^2 - x^2)^2} + \frac{\varepsilon A_s V_{dc}^2 d_w}{(d_w^2 - x^2)^2} \right\} x = \left\{ \frac{\varepsilon A_s V_{dc}}{2(d_n - x)^2} - \frac{\varepsilon A_s V_{dc}}{2(d_w + x)^2} \right\} v_{ac}. \quad (6)$$

There are nonlinear terms of the driving force and the stiffness force in equation (6). Analysis of the nonlinear driving mode vibration can be performed by the Runge–Kutta method. When a driving signal is applied with a frequency near the resonance of the microgyroscope, the vibrating mass is excited with the driving frequency. The output voltage of the monitoring electrode is the final output of the driving mode; the theoretical current i_m that determines the monitoring output V_m can be derived by differentiating the electric charge as

$$i_m = \frac{\varepsilon A_s V_{dc}}{2} \left\{ \frac{1}{(d_n - x)^2} - \frac{1}{(d_w + x)^2} \right\} \dot{x}. \quad (7)$$

The equation of motion of the microgyroscope in the sensing mode vibration can be assumed to be linear. The amplitude of vibration in the y direction can be obtained from equations (2*b*) and (5). If the driving mode vibration is simply sinusoidal, the amplitude of the sensing mode vibration Y induced by the Coriolis force can be written as

$$Y = \frac{2m\omega X\Omega}{[(k_y - k_e - \omega^2 m)^2 + c^2\omega^2]^{1/2}} \quad (8)$$

where ω is the driving frequency. The final output, the voltage of the sensing electrode, is determined by the current i_{sens}, which is the time derivative of the charge stored in the sensing electrodes and can be expressed as

$$i_{sens} = \frac{\mathrm{d}}{\mathrm{d}t}(V_{dc}C_1 - V_{dc}C_2) = \varepsilon A_s V_{dc} \frac{\mathrm{d}}{\mathrm{d}t} \left(\frac{1}{d_n - y} + \frac{1}{d_w + y} - \frac{1}{d_n + y} - \frac{1}{d_w - y} \right). \quad (9)$$

Assuming that d_w is sufficiently larger than d_n and y, equation (9) can be approximated by

$$i_{sens} = \frac{\varepsilon A_s V_{dc}}{2} \left\{ \frac{d_n^2 + y^2}{(d_n^2 - y^2)^2} - \frac{d_w^2 + y^2}{(d_w^2 - y^2)^2} \right\} \dot{y} \approx \left(\frac{\alpha^2 - 1}{\alpha^2} \right) \frac{\varepsilon A_s V_{dc}}{2d_n^2} \dot{y}. \quad (10)$$

From equation (8) and (10), the amplitude of i_{sens} is then given by

$$I_{sens} = \left(\frac{\alpha^2 - 1}{\alpha^2} \right) \frac{\varepsilon A_s V_{dc} m\omega^2 X\Omega}{d_n^2[(k_y - k_e - \omega^2 m)^2 + c^2\omega^2]^{1/2}}. \quad (11)$$

The driving frequency ω is usually selected at the point of the driving mode resonance, which is given as

$$\omega = \left(\frac{k_x - k_e}{m} \right)^{1/2}. \quad (12)$$

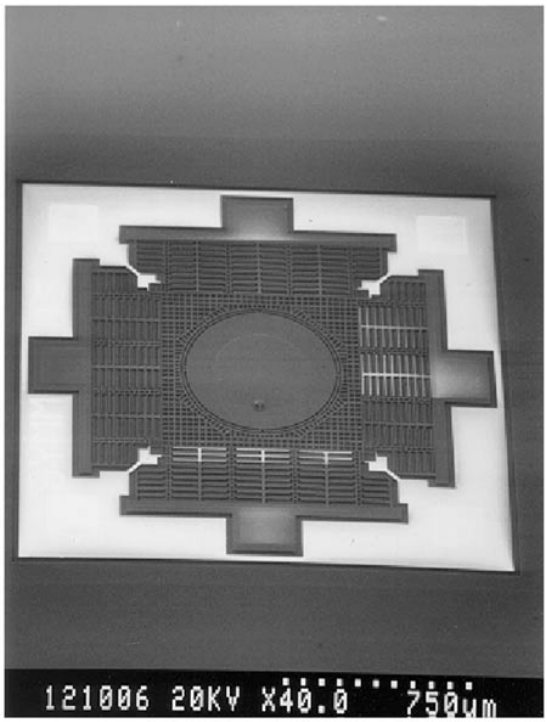

Figure 3. SEM micrograph of the laterally vibrating microgyroscope, which is symmetric about the x- and y-axes.

If the driving frequency is fixed as the frequency of equation (11), using the Q-factor and the detuning ratio γ, equation (10) can be rewritten as

$$I_{sens} = \left(\frac{\alpha^2 - 1}{\alpha^2}\right) \frac{\varepsilon A_s V_{dc} X Q \Omega}{d_n^2 [Q^2(\gamma^2 - 1)^2 + \omega^2]^{1/2}} \tag{13}$$

where the Q-factor represents the vacuum level and γ is defined by the ratio of the sensing resonant frequency to driving resonant frequency

$$\gamma = \left(\frac{k_y - k_e}{k_x - k_e}\right)^{1/2}. \tag{14}$$

The value of γ becomes one if the sensing mode resonant frequency is exactly tuned to the driving mode resonant frequency.

4. Fabrication

An SEM micrograph of the micromachined vibrating gyroscope which is symmetric about the x- and y-axes is shown in figure 3. Figure 4 depicts the fabrication processes for the designed microgyroscope. A low-temperature-oxide (LTO) sacrificial layer of 3 μm thickness, and a polysilicon layer of 5 μm are deposited to form the polysilicon-on-insulator structure. 1 μm of the LTO layer is consecutively deposited and patterned as an anisotropic etching mask. The structural layer of 5 μm is etched by reactive ion etching (RIE), and the surface of the etched structure is doped by $POCl_3$ diffusion followed by an annealing process [8]. An aluminum layer of 300 nm is sputtered, and metal pads are patterned using wet etching. The final structure is released using HF in gas phase etching (GPE), to avoid the stiction problem [9].

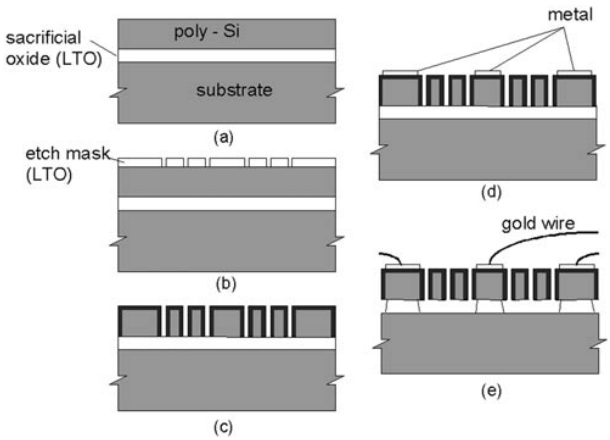

Figure 4. Fabrication steps of a planar vibrating microgyroscope: (a) deposition of polysilicon on insulator; (b) patterning of the etch mask; (c) patterning of the structure layer; (d) patterning of the metal pads; and (e) final structure with attached wiring.

5. Evaluation of the resonator as a gyroscope with self-tuning characteristics

5.1. Evaluation of the dynamic model of the driving mode

The shapes of the driving and sensing electrodes are identical since the resonator is designed to be symmetrical with respect to the x- and y-axes. As mentioned, such a configuration makes it possible to minimize process-induced non-uniformities causing differences between the resonant vibration modes. In the driving electrode, the electrostatic force is a nonlinear function of vibration displacement. Through analysis, a stable and predictable driving range can be obtained. Figure 5 presents a comparison between simulations and experiments which were performed to evaluate the nonlinear driving model. The graphs in figure 5 show the nonlinear vibration in terms of frequency and voltage. The linear parameters of the lumped mass model are the vibrating mass m, the viscous damping coefficient c, and the elastic coefficients k_x and k_y. Of these parameters, m can be approximately calculated from the design dimensions; this value was 6.7042×10^{-9} kg. The elastic coefficients of the resonator can be calculated by measuring the resonant frequency, while the viscous damping coefficient can be obtained by measuring the Q-factor of the resonator. The measured frequency of the selected resonator was 21 323 Hz and the elastic coefficient of the driving mode calculated from the measured resonant frequency was 120.338 N m^{-1}. The viscous damping coefficient c can be estimated with the Q-factor, which is obtained by investigating the frequency response characteristics. The relationship between c and the Q-factor is given by

$$c = \frac{mw}{Q} \tag{15}$$

where ω is the driving frequency at resonance. A test structure with the resonator's dimensions was used for measuring the Q-factor. The measured Q-factor of the test structure was 4815.4 at a pressure of 300 mTorr. Hence, the estimated viscous damping coefficient c of the resonator for microgyroscope was 1.784×10^{-7} N s m^{-1}.

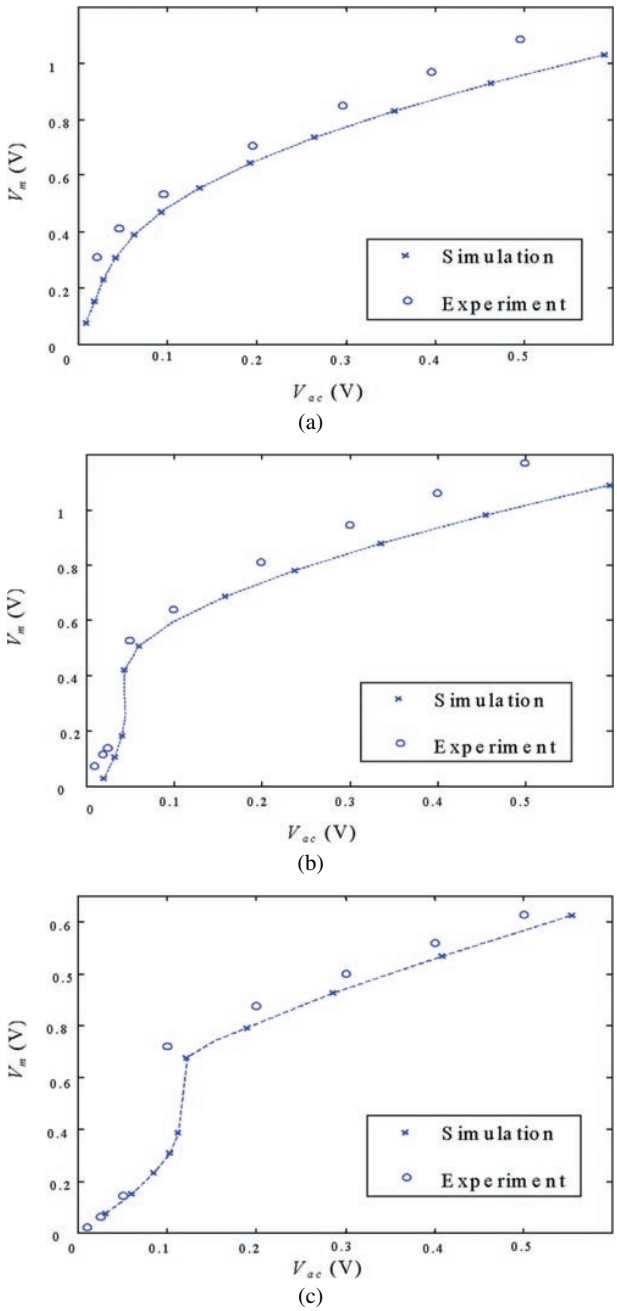

Figure 5. Comparison between the driving mode model and experiment with driving frequencies of: (a) 21 212, (b) 21 211 and (c) 21 210 Hz.

The driving mode vibration of equation (6) and the monitoring current of equation (7) were calculated using the Runge–Kutta method. The dynamic model of the driving mode was evaluated through experiments conducted at a pressure of 100 mTorr and a dc voltage of 5 V, the maximum IC application voltage. The data obtained in the comparison between simulations and experiments on the driving mode vibration is shown in figure 5. The experimental operating conditions were also applied to the simulation. The calculated monitoring output was obtained by multiplying the estimated gain resistance by the analyzed monitoring current. Experiments were performed at three driving frequencies near the driving resonant frequency, namely at 21 212, 21 211 and 21 210 Hz, and the results are shown in figures 5(a), 5(b) and 5(c), respectively. The calculated monitoring output yielded results similar to those obtained in the experiments of nonlinear characteristics and amplitudes. The vibrating amplitude can accordingly be obtained from the evaluated nonlinear analysis.

There is instability in the driving mode of vibration if the driving input is larger than a certain value, which is not shown in figure 5. Data analyzed using the Runge–Kutta method also displayed instability at a certain operational range. In simulation this instability occurred when the ac voltage amplitude was over 2.8 V, whereas in the experiment, the ac voltage amplitude of instability was 2.2 V. The simulated and experimental results of the driving mode vibration were in acceptable agreement. By adjusting the operation conditions within the stable range evaluated through the analysis of the driving model stability in the driving mode is guaranteed.

5.2. Evaluation of the self-tuning characteristics

The sensing mode vibration of the dynamic model was also evaluated. The output voltage proportional to the angular rate can be calculated by multiplying the sensing current from equation (13) by the output gain resistance (in this case 200 MΩ). The experiment on angular rate sensing was also performed using a rate table in a 100 mTorr vacuum chamber. In the output signal, electrical cross-talk from the driving signal to the sensing signal can be observed, and this is due to the parasitic capacitance of the electrodes. There is also mechanical coupling between the primary and secondary motions because the primary motion cannot be perfectly perpendicular to the secondary motion. Thus, the driving vibration at resonance may cause a sensing error, which is independent of the angular rate. The total error signal is a superposition of signals from electrical and mechanical coupling and noises. Since the error signals from electrical and mechanical coupling are independent of the angular rate, they can be easily removed by signal processing using the phase difference between the angular rate and the error signal.

To evaluate the resonator as a gyroscope, the self-tuning capability had to be proved. The ideal microgyroscope in the study features self-tuning characteristics by nature, but detuned frequency actually exists however. The measurements summarized in table 1 represent the resonant frequencies of fabricated resonators. The standard deviations of the resonant frequencies of the primary and secondary modes were 1231.8 and 1214.1 Hz, respectively, but the average difference in the driving and sensing modes was 91.75 Hz, which is less than one-tenth of the standard deviation of resonant frequencies. This proves the self-tuning characteristics in the driving and sensing modes of the resonators. However, frequency differences still exist due to the mentioned inherent limitations in the fabrication process. On the other hand the microgyroscope showed a wide angular rate bandwidth due to the detuning frequency. This bandwidth was over 20 Hz, the limit of the rate table capacity.

Table 1. Eight sets of driving resonant frequencies, sensing resonant frequencies and detuned frequencies.

Sample No	Resonant frequency of primary mode (Hz)	Resonant frequency of secondary mode (Hz)	Detuned frequency (Hz)
1	21 211	21 143	68
2	22 620	22 547	73
3	22 481	22 400	81
4	23 095	23 011	84
5	22 509	22 419	90
6	24 471	24 363	108
7	24 290	24 178	112
8	24 788	24 670	118
Standard deviation of each mode	1231.8	1214.1	
Average of detuned frequency			91.75

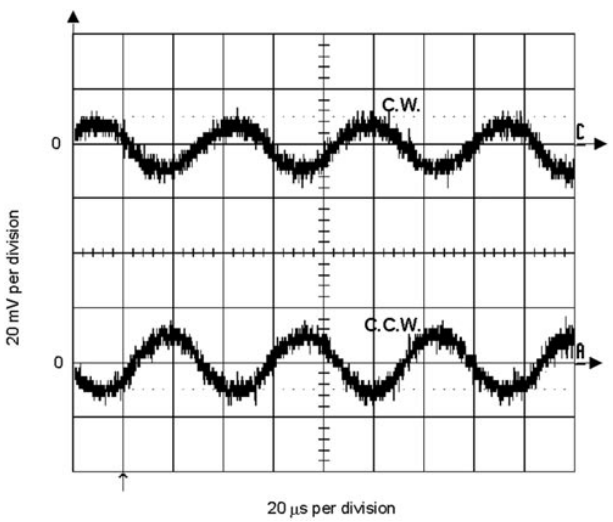

Figure 6. Output signal of the microgyroscope for (a) clockwise (CW) 250 $^\circ$ s^{-1} and (b) counter clockwise (CCW) angular rate 250 $^\circ$ s^{-1}.

The calculated sensitivity of the dynamic model was 2.5 mV s^{-1} under the condition of perfect tuning and pressure of 100 mTorr. The minimum detuned frequency between the driving and sensing mode of the microgyroscope actually measured was 68 Hz, therefore the recalculated sensitivity changed to 0.028 mV s^{-1}. Figure 6 shows the experimental output signal of the microgyroscope at 250 $^\circ$ s^{-1} with a sensitivity of 0.034 mV s^{-1}. Because the simulated and experimental sensitivities show similar values, the modeling of sensing mode vibration can be regarded as acceptable.

6. Summarizing remarks

A laterally driven 2DOF resonator, which is applicable to vibrating microgyroscopes, was proposed. Since this resonator was designed with a symmetrical structure so that it would have identical stiffness in the two orthogonal axes, a microgyroscope using the resonator has self-tuning characteristics. The resonator was fabricated by forming a structure of a single polysilicon layer on an insulator. A dynamic model of the microgyroscope was developed and the validity of this model was evaluated experimentally. The fabricated resonator for microgyroscopic application presents acceptable self-tuning characteristics.

The feasibility of the resonator as a vibrating microgyroscope was discussed. The minimum experimental detuned frequency was 68 Hz with the sensitivity of 0.034 mV s^{-1}. The sensitivity of the microgyroscope is low due to process-induced non-uniformity; however, the angular rate bandwidth is wide. Thus, the resonator could be successfully applied to a vibrating microgyroscope. The results indicate that the development of improved fabrication methods to decrease process errors could increase the sensitivity of the microgyroscope, and that noise levels could be further reduced by the development of improved ICs.

References

[1] Bernstein J, Cho S, King A T, Kourepenis A, Maciel P and Weinberg M 1993 A micromachined comb-drive tuning fork rate gyroscope *Digest IEEE/ASME MicroElectroMechanical Systems Workshop (Fort Lauderdale, FL, February 1993)* pp 143–8

[2] Tanaka K, Mochida Y, Sugimoto S, Moriya K, Hasegawa T, Atsuchi K and Ohwada K 1995 A micromachined vibrating gyroscope *Proc. IEEE MicroElectroMechanical Systems (Amsterdam, The Netherlands, January 1995)* pp 278–81.

[3] Juneau T and Pisano A P 1996 Micromachined dual input axis angular rate sensor *Solid-State Sensor and Actuator Workshop (Hilton Head, SC, June 1996)* pp 299–302

[4] Clark W A, Howe R T and Horowitz R 1996 Surface micromachined Z-axis vibratory rate gyroscope *Solid-State Sensor and Actuator Workshop (Hilton Head, SC, June 1996)* pp 283–7

[5] Hong Y S, Lee J H, Lee C S, Jang W I, Choi C A, Kim S and Kwak Y 1999 Bandwidth analysis of a microgyroscope vibrating in x, y axis and its optimal design *Proc. SPIE, Design, Test, and Microfabrication of MEMS and MOEMS (Paris, April 1999)* vol 3680, pp 939–47

[6] Degani O, Seter D J, Socher E, Kaldor S and Nemirovsky Y 1998 Optimal design and noise consideration of micro machined vibrating rate gyroscope with modulated integrative differential optical sensing *J. MicroElectroMech. Syst.* **7** 329–38

[7] An S, Oh Y S, Lee B L, Park K Y, Kang S J, Choi S O, Go Y I and Song C M 1998 Dual-axis microgyroscope with closed-loop detection *Proc. IEEE MicroElectroMechanical Systems (Heidelberg, Germany, January 1998)* pp 328–33

[8] Choi C A, Lee C S, Jang W I, Hong Y S, Lee J H and Sohn B K 1999 Stress characteristics of multi-layered polysilicon film for the fabrication of micro resonators *Japan. J. Appl. Phys.* **38** 3693–9

[9] Lee J H, Jang W I, Lee C S, Lee Y I, Choi C A, Baek J T and Yoo H J 1998 Characterization of anhydrous HF gas-phase etching with CH_3OH for sacrificial oxide removal *Sensors Actuators* A **64** 27–32